











Fluorination of graphene leads to susceptibility for nanopore formation by highly charged ion impact

S. Creutzburg ^{1,5,*}, M. Mergl,² R. Hübner ¹, I. Jirka ², D. Erb ¹, R. Heller,¹ A. Niggas ³, P. L. Grande ⁴,
F. Aumayr ³, R. A. Wilhelm ³, M. Kalbac ^{2,†} and S. Facsko ^{1,‡}

¹Helmholtz-Zentrum Dresden-Rossendorf, Institute of Ion Beam Physics and Materials Research, 01328 Dresden, Germany, European Union

²J. Heyrovsky Institute of Physical Chemistry of the CAS, v.v.i., 18223 Prague 8, Czech Republic, European Union

³TU Wien, Institute of Applied Physics, 1040 Vienna, Austria, European Union

⁴Federal University of Rio Grande do Sul, Ion Implantation Laboratory, CEP 91501-970 Porto Alegre, Brazil

⁵TU Dresden, 01062 Dresden, Germany, European Union



(Received 13 March 2021; revised 18 June 2021; accepted 8 July 2021; published 26 July 2021)

The formation of nanopores by highly charged ion impacts on freestanding fluorine-functionalized graphene is demonstrated. The process is driven by potential sputtering, which becomes active by changing the semimetallic property of graphene into a strongly insulating state by fluorination. The interaction of fluorographene with highly charged ions is also studied in terms of charge exchange and kinetic energy loss. A higher number of captured electrons and a larger kinetic energy loss than in pristine graphene are observed, which can be well explained by an increase in the ion neutralization length and in the atomic areal density of the target, respectively. Using a computer code based on a time-dependent scattering potential model, a connection between the efficiency of charge exchange and the fluorine coverage is revealed. Our results suggest a competition of two distinct nanostructure formation processes, leading either to pore formation or fluorine desorption.

DOI: [10.1103/PhysRevMaterials.5.074007](https://doi.org/10.1103/PhysRevMaterials.5.074007)

I. INTRODUCTION

Graphene is the most prominent representative of the class of two-dimensional (2D) materials [1]. Since its isolation in 2004 [2], it has received lots of attention in research and applications due to its outstanding properties relevant in optics [3], electronics [4], and photonics [5]. Graphene is distinguished by its ultrahigh electrical conductivity [6], high mechanical strength [7], and superior thermal conductivity [8]. These properties make graphene also a promising candidate for flexible electronics [9]. State-of-the-art chemical vapor deposition (CVD) [10] allows the growth of large-area and almost defect-free graphene. Its availability on a large scale paved the way for industrial applications, e.g., in electronics but also in membrane technologies [11]. Pristine graphene is impermeable to liquids, which makes it an ideal sealing material [12]. The controlled perforation of graphene even extends the application potential and covers fields from water desalination [13], atmospheric filtering [14], molecular separation [15], and catalysis [16] to DNA sequencing [17]. Therefore the production of nanopores with sizes ranging from subnanometers up to a few nanometers is necessary [11]. For pore drilling, commonly techniques relying on ion and electron beams are used [18,19]. Formation of pores with radii in the sub-10-nm range was demonstrated in graphene by the use of focused

electron [20] and helium ion beams [21]. However, these techniques are time-consuming, when large areas are perforated, since high fluences are necessary to produce one single pore, i.e., helium fluences of $\approx 10^5$ ions per nm^2 are required for pore formation [21,22]. Methods based on chemical etching are faster [23]; however, the size of the produced pores is poorly controllable [11].

Recently, highly charged ion (HCI) irradiation was proposed as an efficient technique for the perforation of two-dimensional MoS_2 membranes [24]. By irradiating suspended monolayers of MoS_2 with highly charged xenon ions with charge states between 20 and 40, the authors demonstrated the formation of pores with a mean radius ranging from 0.6 to 2.6 nm, adjustable by the charge state of the ions. Pores of these sizes are well suitable for applications like water desalination or DNA sequencing [11]. Here the efficiency of pore production approaches unity.

Still, the utilization of perforated graphene for membrane technologies would be favorable, since large-scale growth is much easier. However, pore formation in graphene by highly charged ion impacts is not feasible so far, as shown recently [25,26]. In the transmission electron microscope (TEM), no structural damage with respect to nanometer-sized holes was observed after highly charged ion irradiation. This was attributed to the ultrahigh electrical conductivity of graphene, which allows rapid screening of the induced electronic excitations. Also self-healing properties of graphene may close small pores rapidly [27,28]. Insulating carbon nanomembranes instead revealed nanopore formation by highly charged ion impacts [29,30]. Therefore it is obvious that the electronic

*s.creutzburg@hzdr.de

†martin.kalbac@jh-inst.cas.cz

‡s.facsko@hzdr.de

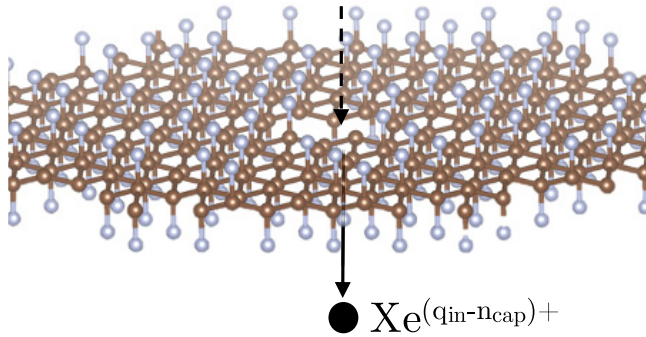


FIG. 1. A highly charged xenon ion with initial charge state q_{in} is transmitted through fluorographene. During neutralization, the ion captures and stabilizes a number of n_{cap} electrons, leading to a reduction of the ion charge state accordingly. Corresponding potential energy deposition in the target and subsequent energy dissipation lead to nanopore formation. Fluorine atoms are shown in blue-gray, carbon atoms in brown.

properties of the target material plays an important role in the nanostructure formation process.

The chemical functionalization [31] of graphene is a promising way to tune its electronic and optical properties. Among different functional groups, fluorine has several advantages. The band gap of fully fluorinated samples can be large (over 3 eV), hence graphene is turned into an insulator [32]. Moreover, the fluorination of graphene is extensively studied and it can be controlled to a large extent [33–35]. Finally, fluorine can be exchanged with a plethora of functional groups, which enables the preparation of graphene membranes with on-demand properties [36].

With respect to the interaction with highly charged ions, the influence of fluorination can be studied by a comparison with experiments for pristine graphene, which was investigated extensively in former works [25,37–39]. For the present study, highly charged xenon ions were transmitted through suspended fluorine-functionalized graphene (Fig. 1). Structural characterization after irradiation was carried out using scanning transmission electron microscopy (STEM). Additionally, exit charge-state spectra of transmitted ions were measured during irradiations. These provided the number of captured and stabilized electrons n_{cap} due to the ions' neutralization by passing the graphene sheet. Thus insights into the neutralization dynamics associated with the deposition of the ion potential energy are gained [40].

II. EXPERIMENT

A. Sample fabrication

Graphene was synthesized by CVD [41,42] on a copper foil (thickness $25\ \mu\text{m}$, purity 99.9%). For growth, the copper foil was loaded into a quartz tubular furnace and annealed at 1000°C in hydrogen flow of 50 sccm for 20 min followed by the injection of methane (CH_4) for 30 min. Afterwards, overgrown graphene domains were etched in hydrogen flow for 5 min. Subsequently, the sample was cooled to 90°C and removed from the furnace. The copper foil was etched from

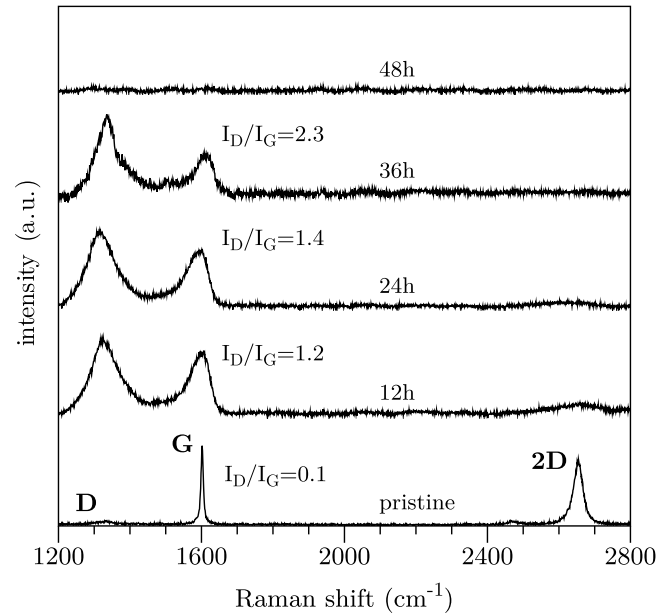


FIG. 2. Raman spectra as a function of fluorination time. Spectra are stacked for better visualization.

the bottom side using a 30% aqueous solution of FeCl_3 and diluted hydrochloric acid.

The as-grown graphene was transferred onto a thermally oxidized Ni/NiO₂ TEM grid (Mesh 2000, 2spi) using a PMMA-supported [poly(methyl methacrylate)] wet-transfer procedure. After transfer, the polymer was removed by acetone vapor. The samples were cleaned by rinsing in isopropyl alcohol and methanol:deionized water, succeeding a blow-drying step with argon.

Suspended graphene was fluorinated by thermal degradation of xenon fluoride (XeF_2) (Aldrich, 99.99%, CAS: 13709-36-9) under autogenous pressure. The samples were fixed on a Teflon jig and stored in a Teflon-lined autoclave, which was loaded by 500 mg of XeF_2 under argon atmosphere. Fluorination was initiated by adjusting the temperature slightly above the critical point of XeF_2 at 120°C , which caused its sublimation followed by the dissociation and subsequent chemisorption of the evolved fluorine radicals on graphene. The calculated vapor pressure of the XeF_2 gas in the reactor amounts to 1.243 bar for a temperature of 120°C [43].

In order to optimize the fluorination process, the samples were investigated as a function of fluorination time by means of Raman spectroscopy. Spectra were acquired immediately after fluorination with a LabRAM HR microscope equipped with a HeNe laser of 633 nm. The laser was focused to a spot size of $1\ \mu\text{m}^2$ on the sample surface using a $100\times$ objective. A laser power of $\sim 1\ \text{mW}$ at the sample surface was achieved in order to minimize the influence of heating. The spectrometer was calibrated before each series of measurements by employing the F_{1g} mode of Si at $520.2\ \text{cm}^{-1}$. Raman spectra measured for as-grown graphene and after fluorination times of 12, 24, 36, and 48 h are shown in Fig. 2. Characteristic D, G, and 2D bands are indicated. For the pristine material, the negligible intensity of the D band at $\approx 1336\ \text{cm}^{-1}$ and the

FWHM of 27 cm^{-1} of the 2D band indicate almost defect-free graphene [44]. After exposure to fluorine, the intensity of the D band is significantly enhanced, implying the chemisorption on graphene [32,45]. This manifests itself in an increase of the peak ratio $I(\text{D})/I(\text{G})$ from 0.1 for pristine graphene to 2.3 after a fluorination time of 36 h.

Furthermore, the position of the D band downshifts from $\approx 1336\text{ cm}^{-1}$ for the pure material to $1324\text{--}1317\text{ cm}^{-1}$ after fluorination due to the induced disorder [44]. For the G mode, however, an upshift from 1584 to 1607 cm^{-1} due to fluorination is observed, in agreement with previous experiments on disordered graphene [44]. All Raman modes disappeared completely after 48 h of fluorination, suggesting a full coverage of graphene with chemisorbed fluorine accompanied by the transformation of planar graphene to a cyclohexane chair structure. Consequently, a fluorination time of 48 h was chosen for sample preparation.

After fabrication, samples were stored in UHV at a pressure of $\sim 10^{-10}$ mbar. The stability of fluorinated graphene in UHV over a storage time of ten days was checked by means of x-ray photoelectron spectroscopy (XPS). The results are given in the Supplemental Material (SM) [46].

B. Irradiation and simulation procedures

Highly charged xenon ions with charge states between 20 and 30 selected by a Wien filter were produced by an electron-beam ion trap (EBIT) [47,48] at kinetic energies of $4.4\text{ keV} \times q_{\text{in}}$, where q_{in} denotes the incoming charge state. Ions were also slowed down to kinetic energies of $0.9\text{ keV} \times q_{\text{in}}$ by means of a deceleration unit. An assembly of electrostatic lenses permits steering of the ion beam into the experimental chamber with a spot size of 1 mm diameter on the target.

For the irradiations, samples were placed on a TEM grid holder with an opening for ion transmission experiments mounted on a four-axis goniometer. Transmitted ions were analyzed with respect to their charge state and kinetic energy by means of an electrostatic analyzer (ESA) with an angular acceptance of 1.0° (full angle) [49,50]. The pressure in the experimental chamber was kept at 1×10^{-9} mbar during the experiments. High-angle annular dark-field scanning transmission electron microscopy (HAADF-STEM) imaging before and after irradiations was performed at 200 kV with a Talos F200X microscope (FEI).

Experimental results regarding the charge exchange are compared with computer simulations based on the TDPO (time-dependent scattering potential) model [39,51]. Details on the theoretical background are given in Ref. [51] and in the SM [46]. The computer code explicitly takes the lattice structure of the target material as well as the experimental conditions (detected scattering angles) into account. A corrugated graphene structure, double-sided functionalized by fluorine in chair configuration [52], was assumed. A random distribution of fluorine vacancies was also considered, which determines the fluorine atomic density or coverage, respectively.

III. RESULTS AND DISCUSSION

A. Nanopore formation

Figures 3(a) and 3(b) show STEM images of fluorographene before and after highly charged ion irradiations,

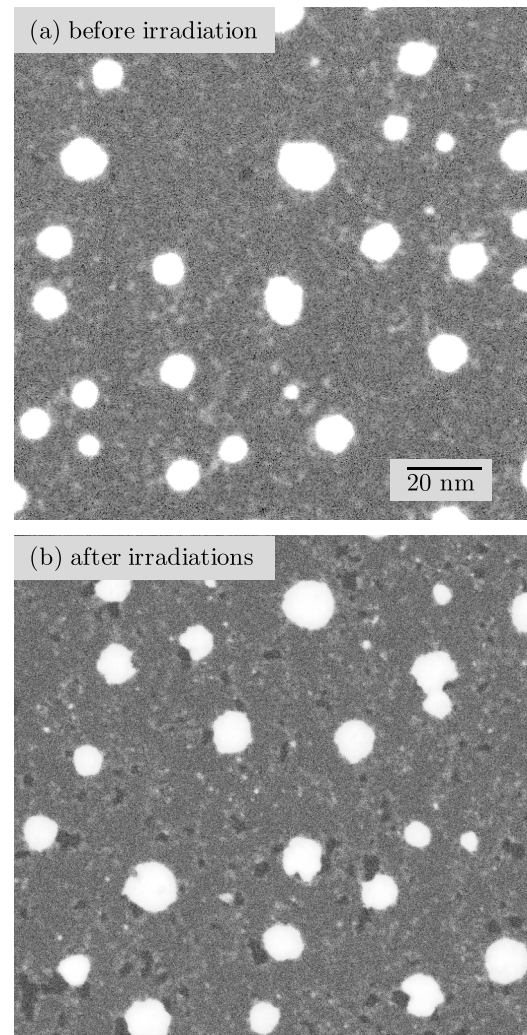


FIG. 3. Examples of STEM images of fluorographene before (a) and after (b) irradiations with highly charged xenon ions. White spots denote iron-containing clusters left from transfer. Darker areas indicate pores. Both images have the same scale bar.

respectively. The irradiations were carried out using various charge states between 20 and 30 and kinetic energies between 20 and 130 keV. Details on the conditions of the irradiation steps (charge state, kinetic energy, and estimated ion fluence) are given in the SM [46]. White spots are clusters of contaminations left from the fabrication process. Element mapping based on energy-dispersive x-ray spectroscopy (performed in the TEM) indicated iron as a main component arising from the FeCl_3 solution [53,54], used as an etchant for the copper foil on which graphene was grown during the preparation process.

In the HAADF-STEM images, dark areas indicate holes in the fluorographene sheet. In order to determine their sizes, the area of each pore was measured using the program IMAGEJ [55] and converted into a radius assuming a circular shape. The distribution of pore density as a function of radius is shown in Fig. 4. The pristine sample shows a total pore density of $1.5 \times 10^{10}\text{ cm}^{-2}$ characterized by a mean pore radius of $(3.1 \pm 1.6)\text{ nm}$. A relative areal coverage of 0.4% for intrinsic holes in the pristine sample is estimated. This is in

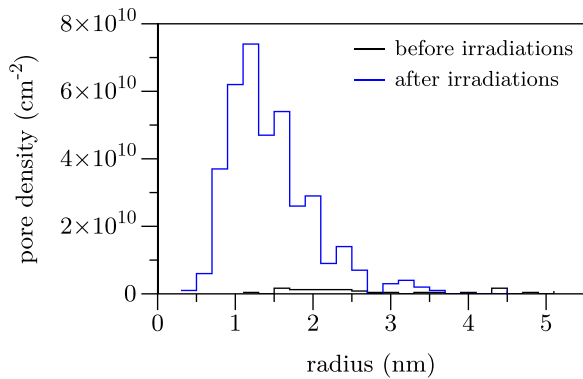


FIG. 4. Distributions of the pore radii before and after highly charged ion irradiations.

fair agreement with Ref. [56], where a value of 0.6% was determined for the areal coverage of intrinsic holes in CVD-grown graphene. There, the formation of intrinsic pores was explained rather as a consequence of the growth process than as an effect of the etching procedure for the growth substrate. No influence of the fluorination process on the formation of intrinsic pores is expected due to the inertness of graphene with respect to chemical functionalization [57] and due to the mild fluorination conditions (pressure and temperature) applied in the present study.

After irradiations, a much higher total pore density of $5.2 \times 10^{11} \text{ cm}^{-2}$ is determined. The higher density is ascribed to ion-induced nanopores. These show smaller radii characterized by a mean value of $(1.5 \pm 0.6) \text{ nm}$, corresponding to a mean sputter yield of 500_{-200}^{+500} atoms. By taking into account the applied ion fluence of $\sim 10^{13} \text{ cm}^{-2}$, an efficiency for pore formation (i.e., the number of pores per ion) of a few percent is estimated. While for pristine graphene no holes were found, applying a fluence of 10^{12} cm^{-2} with even higher charge states of 40 [25,26], the insulating behavior of fluorinated graphene [58] enables the susceptibility to HCI perforation.

Nanopore formation by highly charged ion impact is initiated by the deposition of a fraction of the ion's potential energy associated with charge-exchange processes [30]. Resonant charge transfer from an ion interacting with a solid surface is commonly described by the classical over-the-barrier model [59,60]. In short, an ion approaching a solid surface resonantly captures electrons from the target's surface into highly lying n shells (n indicates the principal quantum number), if a critical distance is reached. A hollow atom is formed characterized by filled outer shells and empty intermediate states [61,62]. When the projectile comes closer to the surface, projectile states with lower quantum numbers n are occupied due to image charge shift and screening of already captured electrons [62]. During the approach to the target surface, transitions of electrons from outer into inner shells already set in by means of autoionization processes [59]; however, the projectile is still strongly excited upon impact [63,64]. Stabilization of excited electrons proceeds to a minor part via the conversion of their excitation energy into x-rays [61].

Most of the ion potential energy is deposited in the target material by means of close impact collisions which facilitate

two-center Auger processes between the projectile and the target atoms [37,39,65,66]. Thereby, a high number of captured electrons on the order of the incident charge state are stabilized and decay into the ground state, proceeding within a femtosecond timescale [25]. For highly charged ion interaction between xenon and carbon, interatomic Coulombic decay [37,67,68] (ICD, similar to direct Auger deexcitation) was proposed as the major relaxation channel of the hollow atom. A comparison between graphene with the 2D semiconductor MoS_2 showed no influence of the electronic properties on the mechanism of potential energy deposition [39].

This is in contrast to the dissipation process of the induced excitations in the material on a later timescale, which determines the efficiency for pore formation. Functionalization of graphene by fluorination leads to an insulating behavior by changing the hybridization from sp^2 into sp^3 [58]. Free electrons become localized due to the attached fluorine atoms and cannot serve as free charge carriers anymore. The induced excitations stay confined on a longer timescale compared to femtoseconds for pure graphene. Therefore a significant fraction of the deposited potential energy will be available for pore formation. Thermal damage formation processes are mediated by electron-phonon coupling heating up the lattice. In the bulk, this can be described within the thermal spike (TS) model [69,70], which was formerly also applied to describe the formation of nanohillocks in CaF_2 by highly charged ion impacts [70,71]. *Ab initio* simulations suggested a high electron-phonon coupling strength in fluorographene [72]. However, nonthermal damage formation processes, like Coulomb explosion (CE) [73,74], bond weakening [75–77], or defect-mediated desorption based on the formation of self-trapped defects [78–81], cannot be ruled out.

B. Charge exchange and kinetic energy loss

The measurement of the ion exit charge state after transmission through the graphene sheet enables the investigation of the timescale of neutralization, which is associated with the potential energy deposition [40]. Figure 5(a) displays the exit charge-state spectrum of Xe^{30+} ions at a kinetic energy of 112 keV transmitted through fluorographene. A spectrum measured for graphene under the same conditions is also shown for comparison. Peaks at high charge states close to $q = 30$, which mark the primary ions, exhibit a shoulder toward lower charge states. This stems from the transmission of ions through cracks and defects in the target on the micrometer scale, leading to only small charge exchange at material edges [37,39]. The distribution at low charge states ($q < 20$) shows a distinct maximum with mean exit charge states of 11 and 15 for fluorographene and graphene, respectively. The lower exit charge state for fluorographene is explained by a larger neutralization length, i.e., a longer ion trajectory in close proximity to the sample, increasing the efficiency for charge exchange (see Fig. 1) From the peak positions of the exit charge states in Fig. 5(a), the kinetic energy loss as a function of the exit charge state was determined and is presented in 5(b). The kinetic energy loss shows an increase toward lower exit charge states, which is well known from highly charged ion interaction with ultrathin foils (e.g., [50,82]). A kinetic energy loss accounting for more than 1000 eV for

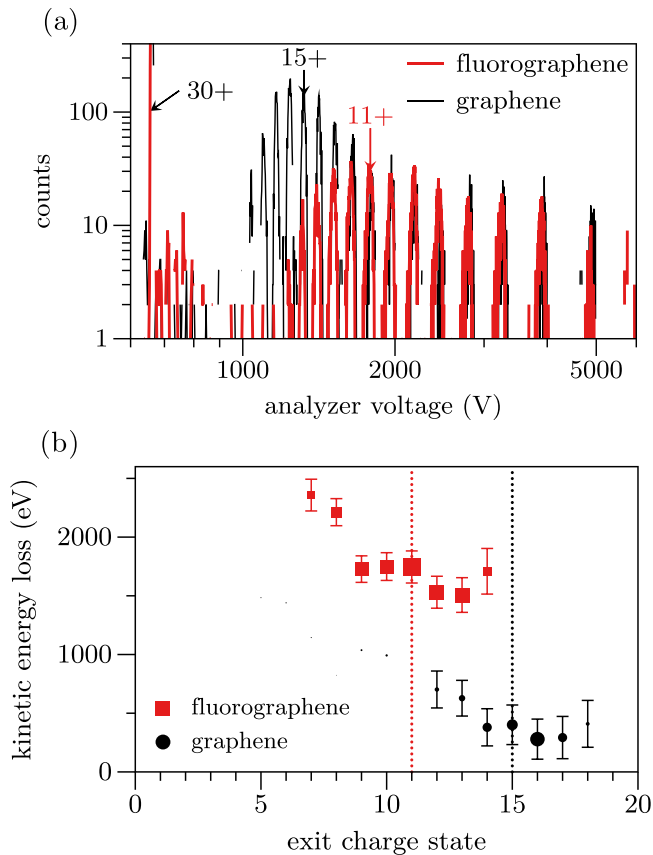


FIG. 5. (a) Exit charge-state spectra of Xe^{30+} ions with an initial kinetic energy of 112 keV transmitted through fluorographene and graphene. Mean exit charge states of 11 and 15, respectively, are indicated. (b) The kinetic energy loss determined from the spectra in (a) is shown for both target materials as a function of the exit charge state. Dashed lines mark the mean exit charge states. The diameter of the symbols indicates the ion abundance.

fluorographene is observed compared to a few hundreds of electronvolts for pristine graphene. Since fluorine atoms attached to the graphene sheet lead to a larger areal atomic density, a higher number of target atoms will be excited upon ion impact. Therefore, larger kinetic energy losses are also expected; however, the band gap prohibits small excitations [83].

Values for the maximum potential energies to be deposited in graphene and fluorographene were also estimated and amount to 13.8 and 14.4 keV, respectively. For this, the expectation value for the potential energy of the transmitted ions was determined by taking into account the relative fractions for the individual exit charge states normalized to the total number of scattered ions. The maximum deposited potential energy is given by the difference between the potential energy of the primary ions and the expectation value for the transmitted ions, neglecting secondary particle emission (see SM [46]). Values for the maximum deposited potential energies are one order of magnitude larger than the respective kinetic energy losses. This shows that ion-induced pore formation is governed by the ion's potential energy deposition rather than its kinetic energy loss.

Ion transmission through iron-containing clusters with radii larger than a few nanometers leads to almost complete

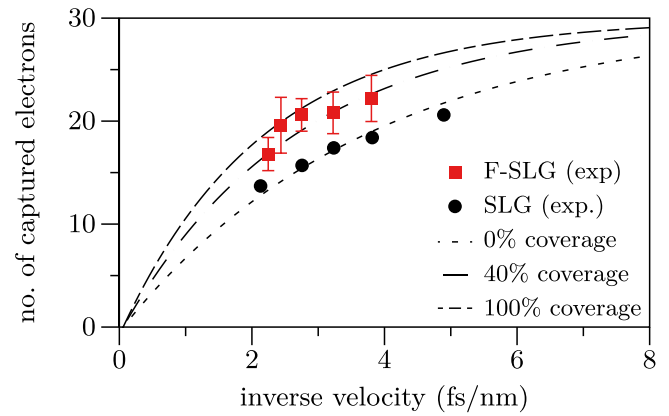


FIG. 6. Number of electrons captured by Xe^{30+} ions over the ion inverse velocity after transmission through fluorographene and graphene. Evaluated spectra were measured within the first 48 h of consecutive irradiations. Lines are added and indicate fits (see text) to the values obtained from TDPT simulations assuming a fluorine coverage of 0%, 40%, and 100%, respectively.

neutralization [84,85]. In this case, exit charge states between 2 and 0 are expected, which are close to the corresponding charge equilibrium values obtained for ion transmission through a thick layer. These are too low for the detection using the ESA. Therefore, ions transmitted through iron clusters do not contribute to the exit charge-state spectra in our measurements.

We measured the charge exchange for Xe^{30+} ions at different initial kinetic energies between 45 and 130 keV and determined the mean exit charge state $\overline{q_{\text{out}}}$ as a function of the ion kinetic energy. The mean number of captured electrons, defined as $q_{\text{in}} - \overline{q_{\text{out}}}$, is shown in Fig. 6 as a function of the ion inverse velocity, which is proportional to the neutralization time. Values for graphene are shown as a reference. Exit charge-state distributions were also simulated by employing the computer code TDPT for different fluorine coverages of a double-sided functionalization. A fluorine coverage of 100% assumes that each carbon atom is partnered with one fluorine atom. Electron capture and deexcitation rates were kept constant for different coverages, because no influence of the electronic target properties on the mechanism of potential energy deposition was observed in previous experiments [39].

The lines in Fig. 6 indicate fits to the number of captured electrons for fluorine coverages of 0% (corresponding to pristine graphene), 40%, and 100% from the simulations. An exponential time dependence for the decay of the ion initial charge state according to $n_{\text{cap}} = (q_{\text{in}} - q_{\text{eq}})[1 - \exp(-\frac{v_N}{v})]$ [86,87] is assumed, where v_N is a neutralization parameter, i.e., the (inverse) charge-state decay constant, and q_{eq} denotes the equilibrium charge state given by $q_{\text{eq}} = Z^{1/3}v/v_0$ [84], which describes the average charge state of an ion with nuclear charge Z passing through a solid with velocity v .

For a fluorine coverage of 0%, a neutralization parameter of 0.27 nm/fs is obtained, fairly resembling the experimental values for pristine graphene. For fluorine coverages of 40% and 100%, the neutralization parameter is enhanced and amounts to 0.38 and 0.47 nm/fs, respectively. In Fig. 6, these values correspond to the lower and upper bounds of the

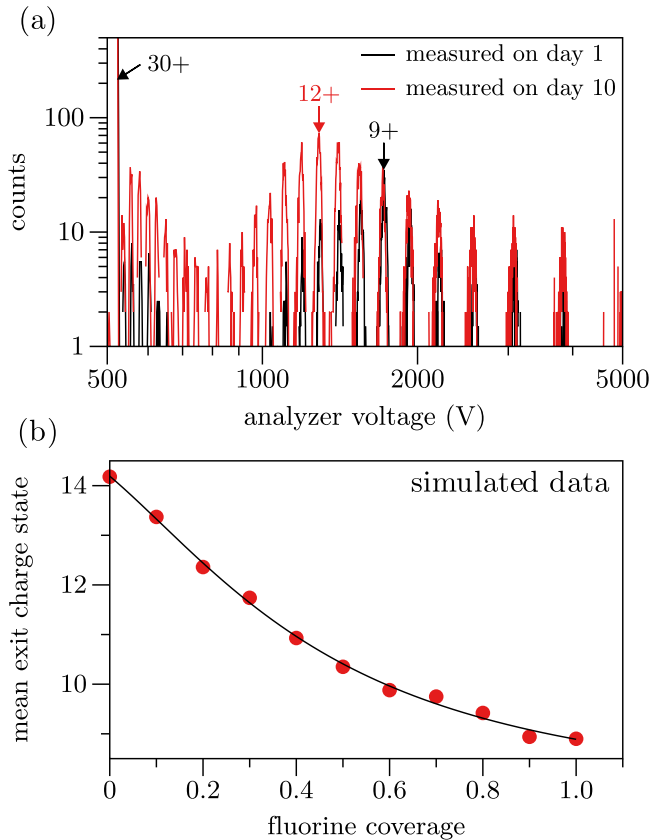


FIG. 7. (a) Experimentally obtained exit charge-state spectra of Xe^{30+} ions at $E_{\text{kin}} = 88$ keV transmitted through fluorographene measured on day 1 and on day 10 of consecutive irradiations. The mean exit charge states of 9 and 12, respectively, are indicated. (b) Dependence of the mean exit charge on the fluorine coverage obtained from TDPO simulations for the same irradiation conditions as given in (a).

s measured values $q_{\text{in}} - \overline{q_{\text{out}}}$. Consequently, a fluorine coverage of $(70 \pm 30)\%$ is estimated.

C. Fluorine desorption during consecutive irradiations

The spectra used for the evaluation in Fig. 6 were measured within the first 48 h after the beginning of irradiations. Exit charge-state spectra were also recorded during consecutive irradiations up to day 10. Figure 7(a) illustrates the spectra measured on days 1 and 10 for Xe^{30+} ions at a kinetic energy of 88 keV. The latter shows a higher number of ions with high charge states $q \geq 20$, which stems from transmission through ion-induced nanopores (see Sec. III A).

Moreover, the mean exit charge state for the lower distribution shifts from $\overline{q_{\text{exit}}} = 9$ on day 1 to $\overline{q_{\text{exit}}} = 12$ on day 10. The increase in the mean exit charge state is ascribed to the desorption of fluorine causing less-efficient charge exchange. In order to investigate the influence of desorption on charge exchange, TDPO simulations were performed, for which the fluorine coverage was gradually varied between 100% and 0%. Figure 7(b) shows the dependence of the mean exit charge state over the fluorine coverage as extracted from the simulations. A monotonic decrease of the fluorine concentration with an increase in the mean exit charge state is seen. A mean exit

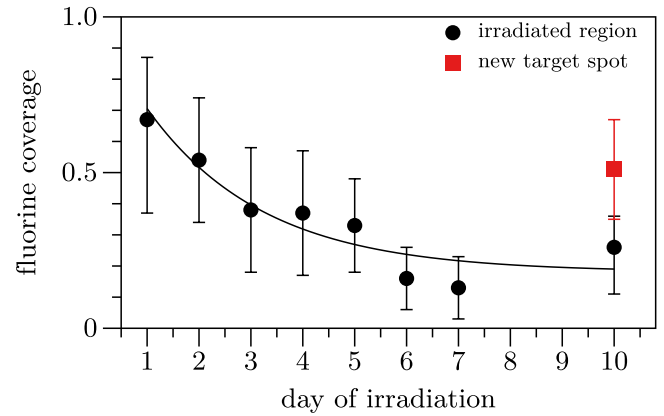


FIG. 8. Time dependence of the relative fluorine coverage estimated by charge-exchange measurements, showing a continuous decrease over time. The solid line was obtained by an exponential fit for eye guiding (see text). On day 10 of the consecutive irradiations, the beam position on the sample was changed to a different target spot, for which a fluorine coverage of $\approx 50\%$ was determined. Compared to the already irradiated region revealing a coverage of $\approx 25\%$, the lower value indicates enhanced fluorine loss due to ion irradiation.

charge state of 9, measured on day 1, would then correspond to a fluorine coverage of $\approx 90\%$, whereas the higher mean exit charge state of 12, measured on day 10, indicates a drop of the fluorine coverage to $\approx 25\%$. Note that the sample is kept at room temperature and UHV conditions throughout the measurements.

We evaluated additional spectra measured on different days taken for different charge states and kinetic energies. Mean exit charge states obtained from the simulations for different fluorine coverages were compared to the experimental data. The values for the coverage, which provided the best agreement in the mean exit charge state between experiment and simulation, are given in the SM [46]. Consequently, from the exit charge-state distributions on different days, the fluorine coverage over time can be extracted, which is shown in Fig. 8. A clear decrease over time is observed, starting from $\approx 70\%$ to $\approx 25\%$ after 10 days of irradiations. Note that consecutive irradiations were performed on the same sample region. After 10 days the ion beam was positioned on a new target spot, for which a higher fluorine coverage of $\approx 50\%$ was determined. This clearly implies enhanced fluorine desorption on the irradiated region.

As an independent and model-free indicator, the kinetic energy loss as a function of exit charge state was determined from the exit charge-state spectra recorded on different days. Mean values for the kinetic energy loss were obtained by taking the average over the exit charge state. For incident Xe^{30+} ions, the velocity dependence of the mean kinetic energy loss, measured for fluorographene within the first 48 h and after 10 days of irradiations, is shown in Fig. 9. Values for graphene were added for comparison. Larger values for fluorographene are observed compared to the pristine material due to the higher atomic areal density of the target. A fit to the experimental data for graphene is obtained based on a proportional dependence of the kinetic energy loss on the

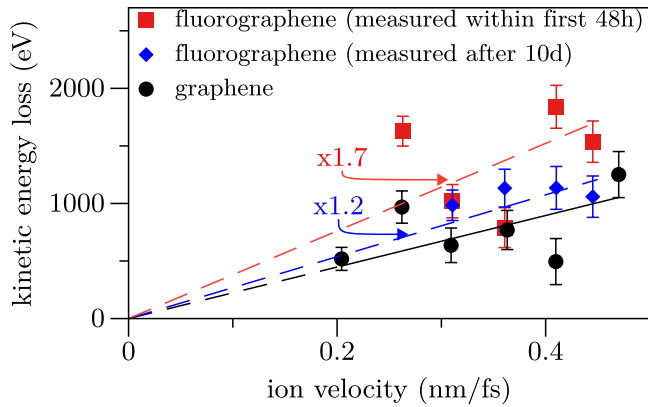


FIG. 9. Velocity dependence of the kinetic energy loss (averaged over the exit charge state) for Xe^{30+} ions transmitted through fluorographene, which was measured within the first 48 h and after 10 days of consecutive irradiations. Values for pristine graphene are shown as reference. The solid line is a fit to the data for graphene, assuming a proportional dependence on the velocity. Dashed lines were obtained by multiplying the fit function with a factor of 1.2 and 1.7, respectively (see text).

velocity. Taking the fitting function for graphene as reference, we estimated values in case of fluorographene considering a 70% higher atomic areal density for the measurements within the first 48 h (i.e., a factor of 1.7 times the energy loss in pristine graphene) and a 20% higher value after 10 days of consecutive irradiations. With respect to the influence of the band gap, no threshold in the kinetic energy loss is ascertained, which would be expected for even lower kinetic energies [83].

For eye guiding, the time dependence of the fluorine coverage in Fig. 8 was described by an exponential function according to $\phi(t) = A \times \exp(-\alpha_{\text{des}} \times t) + C$ [88]. From the fit, we determined a mean desorption rate α_{des} of 0.45 per day and a nondesorbing fraction of 18 %, which indicates nonvolatile and stronger-bound (fluorine) atoms or contaminations remaining attached to the graphene sheet on day 10.

In contrast to the pore formation process described in Sec. III A, defluorination leaves the graphene sheet intact. It is also characterized by a higher cross section compared to perforation. This becomes evident by comparing the relative fractions of the perforated and the defluorinated area of $\approx 4\%$ and $\approx 50\%$, respectively. The disparity is explained by different excitation densities, which are required for the different processes. Fluorine loss proceeds by the dissociation of single-covalent C-F bonds alone. This necessitates lower excitation energies than the ablation of CF clusters for pore formation. Therefore fluorine-depleted regions are also expected close to the rims of ion-induced nanopores, where the density of the induced excitations is lower compared to the impact point.

As a possible underlying mechanism for fluorine loss, defect-mediated desorption is proposed, which explained the loss of halogen atoms due to the irradiation of alkali halides and SiO_2 with photons, electrons, or ions [78–80,89,90]. As shown for LiF [90], defect-mediated desorption is already

efficient at moderate excitation densities, i.e., when multiply charged ions are used (e.g., Ar^{q+} ions, $q \leq 9$, for LiF). It was also applied to describe the creation of nanometer-sized pitlike structures on KBr(001) and KCl(001) surfaces upon highly charged ion impact [81,91]. This process is based on the formation of self-trapped excitons (STEs) upon ion impact [92]. The neutralization of a highly charged ion is accompanied by the formation of electron-hole pairs and hole states in the target surface. In materials with strong electron-photon coupling (like alkali halides or SiO_2), these electronic excitations become localized in a self-produced lattice deformation, leading to the creation of STEs [93]. Relaxation of STEs causes the desorption of the neutralized anions (halide atoms or oxygen). For fluorinated graphene, a strong excitonic response is well known [58,94,95].

IV. CONCLUSIONS AND SUMMARY

Nanopore formation in freestanding fluorographene by highly charged ion impacts is demonstrated and investigated using STEM. Fluorine functionalization alters the electronic properties of originally semimetallic graphene into a highly insulating state. The induced electronic excitations due to the ion impacts remains confined on a timescale longer than femtoseconds for pure graphene, enabling pore formation by potential sputtering. A mean nanopore radius of (1.5 ± 0.6) nm in fluorographene for charge states between 20 and 30 of the incident xenon ions was determined.

Despite the disparity with respect to nanopore formation between fluorine-functionalized and pristine graphene, the process of potential energy deposition is expected to behave similarly. However, the increased target thickness and the larger atomic areal density of fluorographene lead to a higher number of stabilized electrons during the ion's transmission and to a larger kinetic energy loss. A quantitative connection between the mean exit charge state after transmission and the fluorine coverage is shown based on computer simulations, explicitly taking the structural target properties into account. We exploit this dependence to estimate the fluorine coverage using the results of our charge-exchange experiments. Measurements for consecutive irradiations imply fluorine loss, which is considered as a competing process to pore formation. We suggest defect-mediated desorption as the underlying mechanism for fluorine detachment, which is already operative at lower excitation densities. This leads to a higher cross section by one order of magnitude for defluorination compared to pore formation. Depending on the ion charge state, this may allow the use of ion irradiation, either for the modification of the electronic properties [96–98] due to defluorination or for pore formation in graphene [21] as desired for membrane technologies. As detailed in Sec. II A and in the Supplemental Material [46], sample preparation was a complex procedure with low yield. The high sensitivity of fluorinated graphene to environmental influences and aging further limited the amount of suitable sample material. Our aim was therefore to gather as much data as possible from one sample, and indeed all results shown here were obtained from a single sample. On the one hand, this reduces ambiguities with regard to the initial sample properties within the scope of this work so that our observations can reliably be related

to effects of ion charge state and kinetic energy. On the other hand, this fact should certainly encourage further systematic studies investigating different fluorine coverages and irradiation conditions.

ACKNOWLEDGMENTS

Parts of this research were carried out at IBC at the Helmholtz-Zentrum Dresden – Rossendorf e. V., a member

of the Helmholtz Association. We gratefully acknowledge the help and technical support from M. Steinert. Financial support from the Czech Science Foundation (Project No. GACR 20-08633X) and from the Austrian Science Fund (FWF) (Projects No. Y 1174-N36 and No. I 4914-N) is acknowledged. Furthermore, we acknowledge the funding of the TEM Talos by the German Federal Ministry of Education and Research (BMBF) (Grant No. 03SF0451), within the framework of HEMCP.

-
- [1] P. Miró, M. Audiffred, and T. Heine, An atlas of two-dimensional materials, *Chem. Soc. Rev.* **43**, 6537 (2014).
- [2] K. S. Novoselov, A. K. Geim, S. V. Morozov, D. Jiang, Y. Zhang, S. V. Dubonos, I. V. Grigorieva, and A. A. Firsov, Electric field effect in atomically thin carbon films, *Science* **306**, 666 (2004).
- [3] W. Li, B. Chen, C. Meng, W. Fang, Y. Xiao, X. Li, Z. Hu, Y. Xu, L. Tong, H. Wang, W. Liu, J. Bao, and Y. R. Shen, Ultrafast all-optical graphene modulator, *Nano Lett.* **14**, 955 (2014).
- [4] M. F. Craciun, S. Russo, M. Yamamoto, and S. Tarucha, Tuneable electronic properties in graphene, *Nano Today* **6**, 42 (2011).
- [5] F. Bonaccorso, Z. Sun, T. Hasan, and A. C. Ferrari, Graphene photonics and optoelectronics, *Nat. Photonics* **4**, 611 (2010).
- [6] K. I. Bolotin, K. J. Sikes, Z. Jiang, M. Klima, G. Fudenberg, J. Hone, P. Kim, and H. L. Stormer, Ultrahigh electron mobility in suspended graphene, *Solid State Commun.* **146**, 351 (2008).
- [7] C. Lee, X. Wei, J. W. Kysar, and J. Hone, Measurement of the elastic properties and intrinsic strength of monolayer graphene, *Science* **321**, 385 (2008).
- [8] A. A. Balandin, Thermal properties of graphene and nanostructured carbon materials, *Nat. Mater.* **10**, 569 (2011).
- [9] T.-H. Han, H. Kim, S.-J. Kwon, and T.-W. Lee, Graphene-based flexible electronic devices, *Mater. Sci. Eng.: R: Rep.* **118**, 1 (2017).
- [10] K. S. Kim, Y. Zhao, H. Jang, S. Y. Lee, J. M. Kim, K. S. Kim, J. H. Ahn, P. Kim, J. Y. Choi, and B. H. Hong, Large-scale pattern growth of graphene films for stretchable transparent electrodes, *Nature (London)* **457**, 706 (2009).
- [11] T. Yang, H. Lin, X. Zheng, K. P. Loh, and B. Jia, Tailoring pores in graphene-based materials: From generation to applications, *J. Mater. Chem. A* **5**, 16537 (2017).
- [12] J. S. Bunch, S. S. Verbridge, J. S. Alden, A. M. Van Der Zande, J. M. Parpia, H. G. Craighead, and P. L. McEuen, Impermeable atomic membranes from graphene sheets, *Nano Lett.* **8**, 2458 (2008).
- [13] S. P. Surwade, S. N. Smirnov, I. V. Vlassioug, R. R. Unocic, G. M. Veith, S. Dai, and S. M. Mahurin, Water desalination using nanoporous single-layer graphene, *Nat. Nanotechnol.* **10**, 459 (2015).
- [14] S. Blankenburg, M. Bieri, R. Fasel, K. Müllen, C. A. Pignedoli, and D. Passerone, Porous graphene as an atmospheric nanofilter, *Small* **6**, 2266 (2010).
- [15] L. Huang, M. Zhang, C. Li, and G. Shi, Graphene-based membranes for molecular separation, *J. Phys. Chem. Lett.* **6**, 2806 (2015).
- [16] J. Plšek, K. A. Drogowska-Horná, V. L. P. Guerra, J. Mikšátko, V. Valeš, and M. Kalbáč, Towards catalytically active porous graphene membranes with pulsed laser deposited ceria nanoparticles, *Chem. Eur. J.* **27**, 4150 (2021).
- [17] G. F. Schneider, S. W. Kowalczyk, V. E. Calado, G. Pandraud, H. W. Zandbergen, L. M. Vandersypen, and C. Dekker, DNA translocation through graphene nanopores, *Nano Lett.* **10**, 3163 (2010).
- [18] T. Deng, M. Li, Y. Wang, and Z. Liu, Development of solid-state nanopore fabrication technologies, *Sci. Bull.* **60**, 304 (2015).
- [19] H. W. Yoon, Y. H. Cho, and H. B. Park, Graphene-based membranes: Status and prospects, *Philos. Trans. R. Soc. London, Ser. A* **374**, 20150024 (2016).
- [20] M. D. Fischbein and M. Drndić, Electron beam nanosculpting of suspended graphene sheets, *Appl. Phys. Lett.* **93**, 113107 (2008).
- [21] K. Celebi, J. Buchheim, R. M. Wyss, A. Droudian, P. Gasser, I. Shorubalko, J. I. Kye, C. Lee, and H. G. Park, Ultimate permeation across atomically thin porous graphene, *Science* **344**, 289 (2014).
- [22] D. Emmrich, A. Beyer, A. Nadzeyka, S. Bauerdick, J. C. Meyer, J. Kotakoski, and A. Götzhäuser, Nanopore fabrication and characterization by helium ion microscopy, *Appl. Phys. Lett.* **108**, 163103 (2016).
- [23] Z. Fan, Q. Zhao, T. Li, J. Yan, Y. Ren, J. Feng, and T. Wei, Easy synthesis of porous graphene nanosheets and their use in supercapacitors, *Carbon* **50**, 1699 (2012).
- [24] R. Kozubek, M. Tripathi, M. Ghorbani-Asl, S. Kretschmer, L. Madauß, E. Pollmann, M. O'Brien, N. McEvoy, U. Ludacka, T. Susi, G. S. Duesberg, R. A. Wilhelm, A. V. Krasheninnikov, J. Kotakoski, and M. Schleberger, Perforating freestanding molybdenum disulfide monolayers with highly charged ions, *J. Phys. Chem. Lett.* **10**, 904 (2019).
- [25] E. Gruber, R. A. Wilhelm, R. Pétuya, V. Smejkal, R. Kozubek, A. Hierzenberger, B. C. Bayer, I. Aldazabal, A. K. Kazansky, F. Libisch, A. V. Krasheninnikov, M. Schleberger, S. Facksko, A. G. Borisov, A. Arnau, and F. Aumayr, Ultrafast electronic response of graphene to a strong and localized electric field, *Nat. Commun.* **7**, 13948 (2016).
- [26] J. Schwestka, H. Inani, M. Tripathi, A. Niggas, N. McEvoy, F. Libisch, F. Aumayr, J. Kotakoski, and R. A. Wilhelm, Atomic-scale carving of nanopores into a van der Waals heterostructure with slow highly charged ions, *ACS Nano* **14**, 10536 (2020).
- [27] R. Zan, Q. M. Ramasse, U. Bangert, and K. S. Novoselov, Graphene reknits its holes, *Nano Lett.* **12**, 3936 (2012).

- [28] J. Chen, T. Shi, T. Cai, T. Xu, L. Sun, X. Wu, and D. Yu, Self healing of defected graphene, *Appl. Phys. Lett.* **102**, 103107 (2013).
- [29] R. Ritter, R. A. Wilhelm, M. Stöger-Pollach, R. Heller, A. Mücklich, U. Werner, H. Vieker, A. Beyer, S. Facsko, A. Götzhäuser, and F. Aumayr, Fabrication of nanopores in 1 nm thick carbon nanomembranes with slow highly charged ions, *Appl. Phys. Lett.* **102**, 063112 (2013).
- [30] R. A. Wilhelm, E. Gruber, R. Ritter, R. Heller, A. Beyer, A. Turchanin, N. Klingner, R. Hübner, M. Stöger-Pollach, H. Vieker, G. Hlawacek, A. Götzhäuser, S. Facsko, and F. Aumayr, Threshold and efficiency for perforation of 1 nm thick carbon nanomembranes with slow highly charged ions, *2D Mater.* **2**, 035009 (2015).
- [31] G. Bottari, M. Ángeles Herranz, L. Wibmer, M. Volland, L. Rodríguez-Pérez, D. M. Guldi, A. Hirsch, N. Martín, F. D'Souza, and T. Torres, Chemical functionalization and characterization of graphene-based materials, *Chem. Soc. Rev.* **46**, 4464 (2017).
- [32] R. R. Nair, W. Ren, R. Jalil, I. Riaz, V. G. Kravets, L. Britnell, P. Blake, F. Schedin, A. S. Mayorov, S. Yuan, M. I. Katsnelson, H. M. Cheng, W. Strupinski, L. G. Bulusheva, A. V. Okotrub, I. V. Grigorieva, A. N. Grigorenko, K. S. Novoselov, and A. K. Geim, Fluorographene: A two-dimensional counterpart of Teflon, *Small* **6**, 2877 (2010).
- [33] J. Ek Weis, S. D. Costa, O. Frank, Z. Bastl, and M. Kalbac, Fluorination of isotopically labeled turbostratic and Bernal stacked bilayer graphene, *Chem. Eur. J.* **21**, 1081 (2015).
- [34] S. D. Costa, J. E. Weis, O. Frank, M. Fridrichová, Z. Bastl, and M. Kalbac, Do defects enhance fluorination of graphene? *RSC Adv.* **6**, 81471 (2016).
- [35] J. Plšek, K. A. Drogowska, M. Fridrichová, J. Vejpravová, and M. Kalbáč, Laser-ablation-assisted SF₆ decomposition for extensive and controlled fluorination of graphene, *Carbon* **145**, 419 (2019).
- [36] P. Kovaříček, Z. Bastl, V. Valeš, and M. Kalbac, Covalent reactions on chemical vapor deposition grown graphene studied by surface-enhanced raman spectroscopy, *Chem. Eur. J.* **22**, 5404 (2016).
- [37] R. A. Wilhelm, E. Gruber, J. Schwestka, R. Kozubek, T. I. Madeira, J. P. Marques, J. Kobus, A. V. Krasheninnikov, M. Schleberger, and F. Aumayr, Interatomic Coulombic Decay: The Mechanism for Rapid Deexcitation of Hollow Atoms, *Phys. Rev. Lett.* **119**, 103401 (2017).
- [38] A. Niggas, J. Schwestka, S. Creutzburg, T. Gupta, D. Eder, B. C. Bayer, F. Aumayr, and R. A. Wilhelm, The role of contaminations in ion beam spectroscopy with freestanding 2D materials: A study on thermal treatment, *J. Chem. Phys.* **153**, 014702 (2020).
- [39] S. Creutzburg, J. Schwestka, A. Niggas, H. Inani, M. Tripathi, A. George, R. Heller, R. Kozubek, L. Madauß, N. McEvoy, S. Facsko, J. Kotakoski, M. Schleberger, A. Turchanin, P. L. Grande, F. Aumayr, and R. A. Wilhelm, Vanishing influence of the band gap on the charge exchange of slow highly charged ions in freestanding single-layer MoS₂, *Phys. Rev. B* **102**, 045408 (2020).
- [40] P. Ström and D. Primetzhofer, Energy deposition by nonequilibrium charge states of MeV ¹²⁷I in Au, *Phys. Rev. A* **103**, 022803 (2021).
- [41] A. Reina, X. Jia, J. Ho, D. Nezich, H. Son, V. Bulovic, M. S. Dresselhaus, and J. Kong, Large area, few-layer graphene films on arbitrary substrates by chemical vapor deposition, *Nano Lett.* **9**, 30 (2009).
- [42] X. Li, Y. Zhu, W. Cai, M. Borysiak, B. Han, D. Chen, R. D. Piner, L. Colombo, and R. S. Ruoff, Transfer of large-area graphene films for high-performance transparent conductive electrodes, *Nano Lett.* **9**, 4359 (2009).
- [43] F. Schreiner, G. N. McDonald, and C. L. Chernick, Vapor pressure and melting points of xenon difluoride and xenon tetrafluoride, *J. Phys. Chem.* **72**, 1162 (1968).
- [44] A. Eckmann, A. Felten, I. Verzhbitskiy, R. Davey, and C. Casiraghi, Raman study on defective graphene: Effect of the excitation energy, type, and amount of defects, *Phys. Rev. B* **88**, 035426 (2013).
- [45] J. T. Robinson, J. S. Burgess, C. E. Junkermeier, S. C. Badescu, T. L. Reinecke, F. K. Perkins, M. K. Zalalutdniov, J. W. Baldwin, J. C. Culbertson, P. E. Sheehan, and E. S. Snow, Properties of fluorinated graphene films, *Nano Lett.* **10**, 3001 (2010).
- [46] See Supplemental Material at <http://link.aps.org/supplemental/10.1103/PhysRevMaterials.5.074007> for details regarding the results of the XPS measurements, irradiation and simulation procedures, and values for the fluorine coverage as a function of irradiation time.
- [47] G. Zschornack, M. Kreller, V. P. Ovsyannikov, F. Grossman, U. Kentsch, M. Schmidt, F. Ullmann, and R. Heller, Compact electron beam ion sources/traps: Review and prospects (invited), *Rev. Sci. Instrum.* **79**, 02A703 (2008).
- [48] M. Schmidt, H. Peng, G. Zschornack, and S. Sykora, A compact electron beam ion source with integrated Wien filter providing mass and charge state separated beams of highly charged ions, *Rev. Sci. Instrum.* **80**, 063301 (2009).
- [49] R. A. Wilhelm, E. Gruber, V. Smejkal, S. Facsko, and F. Aumayr, Charge-state-dependent energy loss of slow ions. I. Experimental results on the transmission of highly charged ions, *Phys. Rev. A* **93**, 052708 (2016).
- [50] R. A. Wilhelm, E. Gruber, R. Ritter, R. Heller, S. Facsko, and F. Aumayr, Charge Exchange and Energy Loss of Slow Highly Charged Ions in 1 nm Thick Carbon Nanomembranes, *Phys. Rev. Lett.* **112**, 153201 (2014).
- [51] R. A. Wilhelm and P. L. Grande, Unraveling energy loss processes of low energy heavy ions in 2D materials, *Commun. Phys.* **2**, 89 (2019).
- [52] S. S. Han, T. H. Yu, B. V. Merinov, A. C. Van Duin, R. Yazami, and W. A. Goddard, Unraveling structural models of graphite fluorides by density functional theory calculations, *Chem. Mater.* **22**, 2142 (2010).
- [53] B. Alemán, W. Regan, S. Aloni, V. Altoe, N. Alem, C. Girit, B. Geng, L. Maserati, M. Crommie, F. Wang, and A. Zettl, Transfer-free batch fabrication of large-area suspended graphene membranes, *ACS Nano* **4**, 4762 (2010).
- [54] P. Krauß, J. Engstler, and J. J. Schneider, A systematic study of the controlled generation of crystalline iron oxide nanoparticles on graphene using a chemical etching process, *Beilstein J. Nanotechnol.* **8**, 2017 (2017).
- [55] IMAGEJ – An open platform for scientific image analysis, imagej.net/, accessed: 2021-02.25.
- [56] S. C. O'Hern, C. A. Stewart, M. S. H. Boutilier, J.-C. Idrobo, S. Bhaviripudi, S. K. Das, J. Kong, T. Laoui, M. Atieh, and R.

- Karnik, Selective molecular transport through intrinsic defects in a single layer of CVD graphene, *ACS Nano* **6**, 10130 (2012).
- [57] L. Liao, H. Peng, and Z. Liu, Chemistry makes graphene beyond graphene, *J. Am. Chem. Soc.* **136**, 12194 (2014).
- [58] K. J. Jeon, Z. Lee, E. Pollak, L. Moreschini, A. Bostwick, C. M. Park, R. Mendelsberg, V. Radmilovic, R. Kostecki, T. J. Richardson, and E. Rotenberg, Fluorographene: A wide bandgap semiconductor with ultraviolet luminescence, *ACS Nano* **5**, 1042 (2011).
- [59] J. Burgdörfer, P. Lerner, and F. W. Meyer, Above-surface neutralization of highly charged ions: The classical over-the-barrier model, *Phys. Rev. A* **44**, 5674 (1991).
- [60] J. J. Ducrée, F. Casali, and U. Thumm, Extended classical over-barrier model for collisions of highly charged ions with conducting and insulating surfaces, *Phys. Rev. A* **57**, 338 (1998).
- [61] J. P. Briand, L. de Billy, P. Charles, S. Essabaa, P. Briand, R. Geller, J. P. Desclaux, S. Bliman, and C. Ristori, Production of Hollow Atoms by the Excitation of Highly Charged Ions in Interaction with a Metallic Surface, *Phys. Rev. Lett.* **65**, 159 (1990).
- [62] H. Winter and F. Aumayr, Hollow atoms, *J. Phys. B: At., Mol. Opt. Phys.* **32**, R39 (1999).
- [63] D. Kost, S. Facsko, W. Möller, R. Hellhammer, and N. Stolterfoht, Channels of Potential Energy Dissipation during Multiply Charged Argon-Ion Bombardment of Copper, *Phys. Rev. Lett.* **98**, 225503 (2007).
- [64] R. E. Lake, J. M. Pomeroy, H. Grube, and C. E. Sosolik, Charge State Dependent Energy Deposition by Ion Impact, *Phys. Rev. Lett.* **107**, 063202 (2011).
- [65] H. D. Hagstrum, Theory of auger ejection of electrons from metals by ions, *Phys. Rev.* **96**, 336 (1954).
- [66] A. Arnau, F. Aumayr, P. Echenique, M. Grether, W. Heiland, J. Limburg, R. Morgenstern, P. Roncin, S. Schippers, R. Schuch, N. Stolterfoht, P. Varga, T. Zouros, and H. Winter, Interaction of slow multicharged ions with solid surfaces, *Surf. Sci. Rep.* **27**, 113 (1997).
- [67] L. S. Cederbaum, J. Zobeley, and F. Tarantelli, Giant Intermolecular Decay and Fragmentation of Clusters, *Phys. Rev. Lett.* **79**, 4778 (1997).
- [68] T. Jahnke, U. Hergenbahn, B. Winter, R. Dörner, U. Fröhling, P. V. Demekhin, K. Gokhberg, L. S. Cederbaum, A. Ehresmann, A. Knie, and A. Dreuw, Interatomic and intermolecular Coulombic decay, *Chem. Rev.* **120**, 11295 (2020).
- [69] M. Toulemonde, C. Dufour, and E. Paumier, Transient thermal process after a high-energy heavy-ion irradiation of amorphous metals and semiconductors, *Phys. Rev. B* **46**, 14362 (1992).
- [70] C. Lemell, A. El-Said, W. Meissl, I. Gebeshuber, C. Trautmann, M. Toulemonde, J. Burgdörfer, and F. Aumayr, On the nanohillock formation induced by slow highly charged ions on insulator surfaces, *Solid-State Electron.* **51**, 1398 (2007).
- [71] A. S. El-Said, R. Heller, W. Meissl, R. Ritter, S. Facsko, C. Lemell, B. Solleder, I. C. Gebeshuber, G. Betz, M. Toulemonde, W. Möller, J. Burgdörfer, and F. Aumayr, Creation of Nanohillocks on CaF₂ Surfaces by Single Slow Highly Charged Ions, *Phys. Rev. Lett.* **100**, 237601 (2008).
- [72] S. Bruzzone and G. Fiori, Ab-initio simulations of deformation potentials and electron mobility in chemically modified graphene and two-dimensional hexagonal boron-nitride, *Appl. Phys. Lett.* **99**, 222108 (2011).
- [73] I. S. Bitenski and E. S. Parilis, Shock wave mechanism for cluster emission and organic molecule desorption under heavy ion bombardment, *Nucl. Instrum. Methods Phys. Res., Sect. B* **21**, 26 (1987).
- [74] I. S. Bitenski and E. S. Parilis, The sputtering of non-metals under slow multiply charged ions, *J. Phys. Colloques* **50**, C2-227 (1989).
- [75] J. V. Vechten, R. Tsu, F. Saris, and D. Hoonhout, Reasons to believe pulsed laser annealing of Si does not involve simple thermal melting, *Phys. Lett. A* **74**, 417 (1979).
- [76] P. Stampfli, Electronic excitation and structural stability of solids, *Nucl. Instrum. Methods Phys. Res., Sect. B* **107**, 138 (1996).
- [77] T. Schenkel, A. V. Hamza, A. V. Barnes, D. H. Schneider, J. C. Banks, and B. L. Doyle, Ablation of GaAs by Intense, Ultrafast Electronic Excitation from Highly Charged Ions, *Phys. Rev. Lett.* **81**, 2590 (1998).
- [78] M. Szymonski, Electronic sputtering of alkali halides, *Mat. Fys. Medd. K. Dan. Vidensk. Selsk.* **43**, 495 (1993).
- [79] B. Such, J. Kolodziej, P. Czuba, P. Piatkowski, P. Struski, F. Krok, and M. Szymonski, Surface Topography Dependent Desorption of Alkali Halides, *Phys. Rev. Lett.* **85**, 2621 (2000).
- [80] M. Sporn, G. Libiseller, T. Neidhart, M. Schmid, F. Aumayr, H. P. Winter, P. Varga, M. Grether, D. Niemann, and N. Stolterfoht, Potential Sputtering of Clean SiO₂ by Slow Highly Charged Ions, *Phys. Rev. Lett.* **79**, 945 (1997).
- [81] R. Heller, S. Facsko, R. A. Wilhelm, and W. Moller, Defect Mediated Desorption of the KBr(001) Surface Induced by Single Highly Charged Ion Impact, *Phys. Rev. Lett.* **101**, 096102 (2008).
- [82] T. Schenkel, M. A. Briere, A. V. Barnes, A. V. Hamza, K. Bethge, H. Schmidt-Böcking, and D. H. Schneider, Charge State Dependent Energy Loss of Slow Heavy Ions in Solids, *Phys. Rev. Lett.* **79**, 2030 (1997).
- [83] S. N. Markin, D. Primetzhofer, and P. Bauer, Vanishing Electronic Energy Loss of Very Slow Light Ions in Insulators with Large Band Gaps, *Phys. Rev. Lett.* **103**, 113201 (2009).
- [84] N. Bohr, The penetration of atomic particles through matter, *Mat. Fys. Medd. K. Dan. Vidensk. Selsk.* **18**, 116 (1948).
- [85] G. Schiwietz and P. Grande, Improved charge-state formulas, *Nucl. Instrum. Methods Phys. Res., Sect. B* **175-177**, 125 (2001).
- [86] W. Brandt, R. Laubert, M. Mourino, and A. Schwarzschild, Dynamic Screening of Projectile Charges in Solids Measured by Target X-Ray Emission, *Phys. Rev. Lett.* **31**, 1095 (1973).
- [87] M. Hattass, T. Schenkel, A. V. Hamza, A. V. Barnes, M. W. Newman, J. W. McDonald, T. R. Niedermayr, G. A. Machicoane, and D. H. Schneider, Charge Equilibration Time of Slow, Highly Charged Ions in Solids, *Phys. Rev. Lett.* **82**, 4795 (1999).
- [88] B. Tee, M. Vos, H. Trombini, F. Selau, P. Grande, and R. Thomaz, The influence of radiation damage on electrons and ion scattering measurements from PVC films, *Radiat. Phys. Chem.* **179**, 109173 (2021).
- [89] B. Such, P. Czuba, P. Piatkowski, and M. Szymonski, AFM studies of electron-stimulated desorption process of KBr(001) surface, *Surf. Sci.* **451**, 203 (2000).
- [90] T. Neidhart, F. Pichler, F. Aumayr, H. P. Winter, M. Schmid, and P. Varga, Potential Sputtering of Lithium Fluoride by Slow Multicharged Ions, *Phys. Rev. Lett.* **74**, 5280 (1995).

- [91] R. A. Wilhelm, R. Heller, and S. Facsko, Slow highly charged ion induced nanopit formation on the KCl(001) surface, *Europhys. Lett.* **115**, 43001 (2016).
- [92] F. Aumayr, J. Burgdörfer, G. Hayderer, P. Varga, and H. P. Winter, Evidence against the “Coulomb explosion” model for desorption from insulator surfaces by slow highly charged ions, *Phys. Scr.* **T80**, 240 (1999).
- [93] R. Williams and K. Song, The self-trapped exciton, *J. Phys. Chem. Solids* **51**, 679 (1990).
- [94] W. Wei and T. Jacob, Electronic and optical properties of fluorinated graphene: A many-body perturbation theory study, *Phys. Rev. B* **87**, 115431 (2013).
- [95] F. Karlický and M. Otyepka, Band gaps and optical spectra from single- and double-layer fluorographene to graphite fluoride: Many-body effects and excitonic states, *Ann. Phys.* **526**, 408 (2014).
- [96] S. E. Martins, F. Withers, M. Dubois, M. F. Craciun, and S. Russo, Tuning the transport gap of functionalized graphene via electron beam irradiation, *New J. Phys.* **15**, 033024 (2013).
- [97] F. Withers, T. H. Bointon, M. Dubois, S. Russo, and M. F. Craciun, Nanopatterning of fluorinated graphene by electron beam irradiation, *Nano Lett.* **11**, 3912 (2011).
- [98] H. Li, T. Duan, S. Haldar, B. Sanyal, O. Eriksson, H. Jafri, S. Hajjar-Garreau, L. Simon, and K. Leifer, Direct writing of lateral fluorographene nanopatterns with tunable bandgaps and its application in new generation of moiré superlattice, *Appl. Phys. Rev.* **7**, 011403 (2020).